



A Young White Dwarf Orbiting PSR J1835–3259B in the Bulge Globular Cluster NGC 6652

Jianxing Chen^{1,2} , Mario Cadelano^{1,2} , Cristina Pallanca^{1,2} , Francesco R. Ferraro^{1,2} , Barbara Lanzoni^{1,2} , Alina G. Istrate³ , Marta Burgay⁴ , Paulo C. C. Freire⁵ , Tasha Gautam⁶ , Andrea Possenti⁴ , and Alessandro Ridolfi^{4,5}

¹ Dipartimento di Fisica e Astronomia “Augusto Righi,” Alma Mater Studiorum Università di Bologna, via Piero Gobetti 93/2, I-40129 Bologna, Italy; jianxing.chen2@unibo.it

² INAF-Osservatorio di Astrofisica e Scienze dello Spazio di Bologna, Via Piero Gobetti 93/3 I-40129 Bologna, Italy

³ Department of Astrophysics/IMAPP, Radboud University Nijmegen, P.O. Box 9010, NL-6500 GL Nijmegen, The Netherlands

⁴ INAF—Osservatorio Astronomico di Cagliari, via della Scienza 5, I-09047 Selargius (CA), Italy

⁵ Max-Planck-Institut für Radioastronomie MPIfR, Auf dem Hügel 69, D-53121 Bonn, Germany

⁶ National Radio Astronomy Observatory, 520 Edgemont Rd., Charlottesville, VA 22903, USA

Received 2023 February 14; revised 2023 March 17; accepted 2023 March 18; published 2023 May 10

Abstract

We report on the discovery of the companion star to the millisecond pulsar PSR J1835–3259B in the Galactic globular cluster NGC 6652. Taking advantage of deep photometric archival observations acquired through the Hubble Space Telescope in near-UV and optical bands, we identified a bright and blue object at a position compatible with that of the radio pulsar. The companion is located along the helium-core white dwarf cooling sequence, and the comparison with binary evolution models provides a mass of $0.17 \pm 0.02 M_{\odot}$, a surface temperature of $11,500 \pm 1900$ K, and a very young cooling age of only 200 ± 100 Myr. The mass and the age of the companion are compatible with a progenitor star of about $0.87 M_{\odot}$, which started transferring mass to the primary during its evolution along the subgiant branch and stopped during the early red giant branch phase. Combining together the pulsar mass function and the companion mass, we found that this system is observed at an almost edge-on orbit and hosts a neutron star with a mass of $1.44 \pm 0.06 M_{\odot}$, thus suggesting a highly nonconservative mass accretion phase. The young age of the WD companion is consistent with the scenario of a powerful, relatively young MSP indicated by the earlier detection of gamma-rays from this system.

Unified Astronomy Thesaurus concepts: Millisecond pulsars (1062); Binary pulsars (153); Globular star clusters (656); HST photometry (756); Neutron stars (1108); White dwarf stars (1799)

1. Introduction

Millisecond pulsars (MSPs) are rapidly spinning neutron stars (NSs) with periods less than 30 ms (Lyne & Graham-Smith 1998) that are distinguished from the population of “normal” pulsars (Lyne & Graham-Smith 1998), which have longer spin periods. Since the first MSP was discovered in the globular cluster (GC) M28 in 1987 (Lyne et al. 1987), a further 278 MSPs have been discovered in 38 Galactic GCs so far.⁷ More than half of these MSPs are located in a binary system. Although ~ 600 MSPs have been discovered in the Milky Way,⁸ more than one-third of them are hosted by GCs, thus suggesting a link between the MSP formation rate and the environment in which they are formed. In fact, GCs are collisional systems where the high stellar densities and frequent dynamic interactions favor the formation of a large number of exotic objects such as MSPs (e.g., Ransom et al. 2005; Freire et al. 2017; Cadelano et al. 2018; Ridolfi et al. 2022), blue straggler stars (e.g., Ferraro et al. 1993, 1997a, 1999, 2004; Cadelano et al. 2022), and cataclysmic variables (e.g., Rivera Sandoval et al. 2018; Belloni et al. 2019, 2020). Therefore,

GCs provide the ideal stellar laboratories to study the formation and evolution of exotic systems, as well as the complex interplay between stellar evolution and dynamics (Ferraro et al. 2009, 2012; Dalessandro et al. 2013a; Cadelano et al. 2017a; Ferraro et al. 2018, 2019; Lanzoni et al. 2019; Ferraro et al. 2020; Libralato et al. 2022).

MSPs are generally considered the outcome of the evolution of low-mass X-ray binaries (LMXBs) with an NS primary (see Bhattacharya & van den Heuvel 1991; Wijnands & van der Klis 1998; Ferraro et al. 2015). According to this scenario, a slowly rotating NS is spun up through mass accretion and angular momentum transfer from an evolving companion star. At the end of a $\lesssim 1$ Gyr long accretion phase, an exhausted and envelope-stripped companion star is left, commonly a He-core white dwarf (WD; Driebe et al. 1998; Tauris & Savonije 1999; Ferraro et al. 2003a; Istrate et al. 2014; Cadelano et al. 2015b; Antoniadis et al. 2016a). A different class of binary MSPs in tight orbits with period < 1 day are called “spider” MSPs (Roberts 2013). They are characterized by having nondegenerate companion stars that are usually tidally distorted and heated by the interaction with the pulsar and its relativistic wind (Douglas et al. 2022). The formation of MSPs can also be explained through alternative channels such as the accretion-induced collapse (AIC) of a massive oxygen–neon or oxygen–neon–magnesium WD. These systems should be characterized by large orbital periods (Nomoto 1987; Tauris et al. 2013; Freire & Tauris 2014; Tauris et al. 2017; Ablimit et al. 2022; Wang et al. 2022).

⁷ Pulsars in GCs: <http://www.naic.edu/~pfreire/GCpsr.html>.

⁸ The ATNF pulsar catalog: <https://www.atnf.csiro.au/research/pulsar/psrcat/>.



In most cases, MSPs are expected to form in the LMXB channel. Mass accretion during this phase can in principle produce NSs with masses higher than standard slowly rotating pulsars. Therefore, MSPs studies can provide a tool to determine through observations the NS mass distribution and maximum mass sustainable by an NS, which is one of the most valuable parameters to constrain the equation of state of ultradense matter (see Lattimer 2012; Antoniadis et al. 2016a; Özel & Freire 2016).

We are leading a long-term program aimed at identifying MSPs in GCs through near-UV to near-IR photometric and spectroscopic observations of their companion stars with the aim of obtaining a complementary view of the binary properties and studying their formation and evolution in the ideal GC laboratory. This program led to the discovery and characterization of several He-core WD companions (Ferraro et al. 2003a; Cadelano et al. 2015b, 2019), one of them possibly orbiting a high-mass NS (Cadelano et al. 2020), and several companions to spider MSPs (Ferraro et al. 2001b; Sabbi et al. 2003a, 2003b; Cocozza et al. 2006; Pallanca et al. 2010; Mucciarelli et al. 2013; Pallanca et al. 2013, 2014; Cadelano et al. 2015a, 2017b).

Here we report on the identification and characterization of the companion star to NGC 6652B based on high-resolution near-UV and optical observations obtained from the Hubble Space Telescope (HST).

NGC 6652 is a GC located around 10 kpc from the Sun (Harris 1996, 2010 edition), with an age of 13.25 ± 0.5 Gyr (Dotter et al. 2010), an intermediate metallicity of $[\text{Fe}/\text{H}] \approx -0.75$, and a small extinction of $E(B - V) = 0.09$ (Harris 1996, 2010 edition) for a stellar system located in the Galactic bulge. PSR J1835–3259A was the first binary MSP discovered in the cluster by DeCesar et al. (2015), and it is characterized by a pulse period of 3.89 ms, an orbital period of 9.25 days, and a very high eccentricity $e = 0.97$. The MSP is orbiting a companion with a minimum mass of about $0.7 M_{\odot}$, which could be either a massive WD or a secondary NS. This system is likely formed through an exchange encounter in the dense cluster environment. Recently, a new binary MSP, namely J1835–3259B (hereafter NGC 6652B), has been discovered by Gautam et al. (2022). The NS is spinning at 1.83 ms and is located in a 1.2-day-long orbit with an extremely small eccentricity of about 3×10^{-5} . Zhang et al. (2022) used observations obtained by the Fermi Gamma-ray Space Telescope and detected a high-energy emission of the MSP as a source with a γ -ray luminosity of $5 \times 10^{34} \text{ erg}^{-1}$.

This paper is organized as follows: in Section 2, we describe the data set and data reduction; the identification and characterization of the companion star are presented in Section 3; and the conclusions are finally drawn in Section 4.

2. Data Reduction

In this work, we used high-resolution and deep photometric data acquired with the HST in the near-UV band, captured by the UVIS channel of the Wide Field Camera 3 (WFC3); the obtained archival data set is a part of the HST legacy survey of galactic GCs under GO-13297 (PI: Piotto). There are three different filters used: F275W (near-UV), F336W (U), and F438W (B); the observational log of the data set is listed in Table 1.

The data reduction was performed on the calibrated images with extension `_flc` (UVIS calibrated exposure including charge

Table 1
Observation Log of the Data Set

Obs. ID	F275W	F336W	F438W
GO-13297	690s \times 2 775s \times 2 800s \times 2	305s \times 2 313s \times 1 313s \times 3	60s \times 1 69s \times 1 86s \times 1

transfer efficiency correction), after pre-reduction including pixel area map correction.

In searching for the optical companion to PSR J1835–3259A and PSR J1835–3259B, we adopted the so-called “UV-route,” a photometric procedure specifically optimized for the identification of blue and hot objects in crowded fields such as hot horizontal branch stars, blue straggler stars, and WDs and widely used by our group in previous papers (see Ferraro & Paresce 1993; Ferraro et al. 1997a, 1997b, 2001a, 2003b; Dalessandro et al. 2013b). Specifically, in this paper we followed the approach described in Cadelano et al. (2019, 2020; see also Raso et al. 2017, 2020; Chen et al. 2021, 2022).

As the first step, about 250 bright and unsaturated stars were selected to model the point-spread function (PSF) for each image, and then the resulting models were applied to all the sources detected above 4σ from the background. As a second step, we created a “master list” of stars containing all the sources detected in at least half the F275W images. The PSF fitting of all the sources in the master list was forced at the corresponding positions in all the frames using DAOPHOT/ALLFRAME (Stetson 1994). Finally, magnitudes obtained for different stars were averaged and homogenized using DAOPHOT/DAOMASTER.

The instrumental magnitudes were calibrated to the VEGA-MAG system by using appropriate zero-points and aperture corrections.⁹ After correction for geometric distortions (Bellini et al. 2011), the coordinates were aligned to the International Celestial Reference System by cross-correlation with the Gaia DR3 Catalog (Gaia Collaboration et al. 2022). To this aim, we used the cross-correlation software CataXcorr¹⁰ adopting a six-parameter linear transformation to convert the instrumental (x , y) positions to the (R.A., decl.) absolute coordinate system. The transformation residuals returned a combined astrometric uncertainty of about 14 mas.

3. The Companion to NGC 6652B

3.1. Identification of the Companion Star

To identify the optical counterpart of the MSPs in the cluster, we carefully analyzed all the stars in the region surrounding the two MSP positions. No stars are found at a position compatible with PSR J1835–3259A, and we provide the finding chart and magnitude upper limits for this object in Appendix. On the other hand, a peculiar bright and blue star is found at 30 mas from the timing position of NGC 6652B. The resulting 1σ radio timing and optical uncertainty for this MSP is 17 mas (see Section 2 and Table 3 in Gautam et al. 2022); therefore, the two positions of the two sources turn out to be compatible within 1.8σ . Figure 1 shows the finding chart in the three different

⁹ <https://www.stsci.edu/hst/instrumentation/wfc3/data-analysis/photometric-calibration>

¹⁰ <http://daveide2.bo.astro.it/~paolo/Main/CataPack.html>

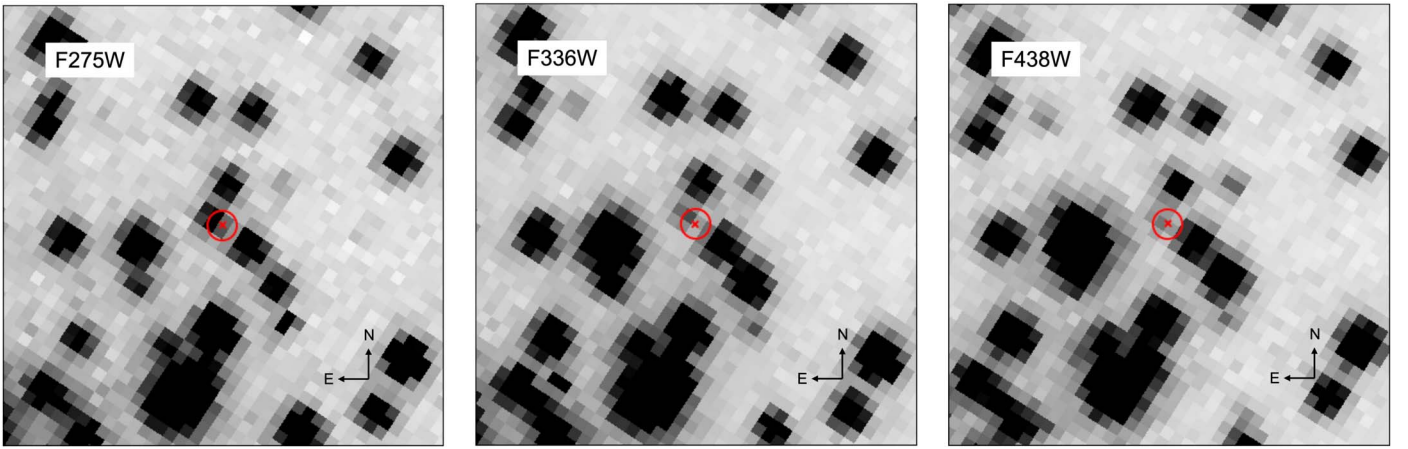


Figure 1. $1''.5 \times 1''.5$ finding chart of the NGC 6652B companion in the F275W, F336W, and F438W filters. The red circle has a radius of 50 mas ($\sim 3\sigma$ uncertainty), while the center of the circle corresponds to the position of the MSP. It is clear that the candidate counterpart (a WD) gets fainter in redder filters, while most of the other stars get brighter.

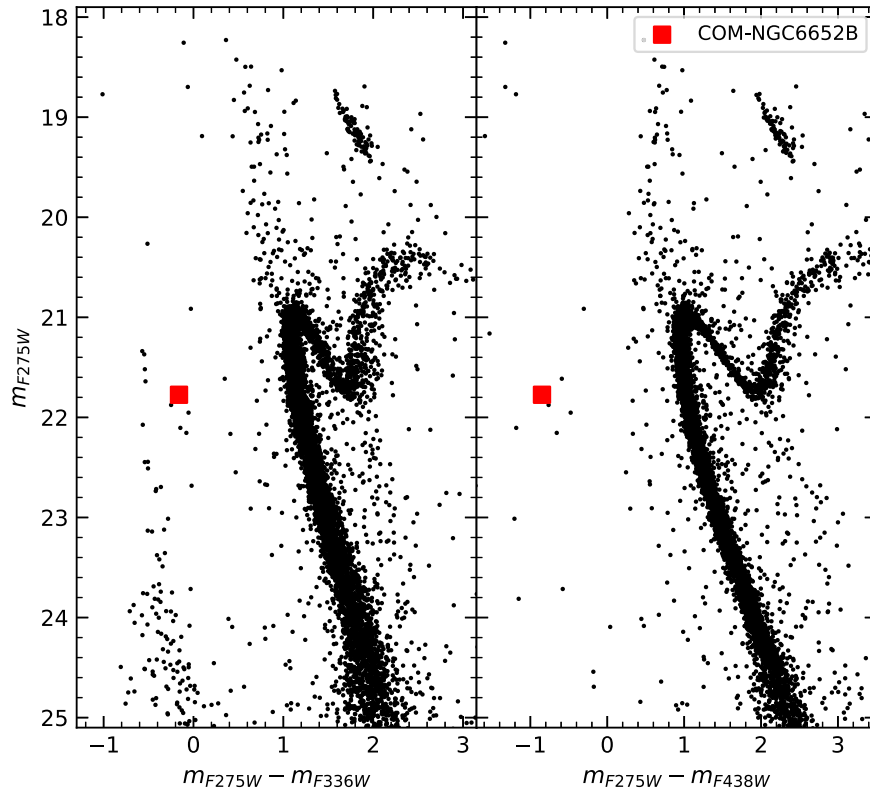


Figure 2. CMDs of NGC 6652. Left and right panels are $(m_{F275W} - m_{F336W}, m_{F275W})$ and $(m_{F275W} - m_{F438W}, m_{F275W})$ filter combinations, respectively. The He-core WD companion to NGC 6652B is marked with a red square in each panel. The error bars are smaller than the red squares.

adopted filters. It can be easily appreciated that the source closest to NGC 6652B is a very blue star, as its luminosity rapidly decreases in redder filters. Nonetheless, the candidate is bright enough to be detected in all three filters with small uncertainties: $m_{F275W} = 21.77 \pm 0.02$, $m_{F336W} = 21.93 \pm 0.04$, and $m_{F438W} = 22.62 \pm 0.07$. Observations in the F606W and F814W filters are available in the HST archive, but we did not include them in the analysis since the companion is not detectable owing to a nearby heavily saturated star that totally hampers any meaningful estimate of the candidate magnitudes in these filters.

Figure 2 shows the color–magnitude diagram (CMD) of the cluster in two different filter combinations. Indeed, in both the

color combinations shown in Figure 2, the candidate companion star (highlighted with a large red square) is located in the CMD region between the main sequence and the CO-WD cooling sequence (which is clearly visible in the left panel at color $m_{F275W} - m_{F336W} < 0$). Considering the photometric errors, its position turns out to be incompatible (at more than 10σ) with both the MS and the CO-WD cooling sequence. On the other hand, this is the portion of the CMD where the He-WD cooling sequences are expected to lie. These WDs are the standard outcome of the mass transfer processes and typically found to be orbiting MSPs. Moreover, due to its luminosity, we can also expect that this is a relatively young WD. Thus, on the basis of its peculiar position in the CMD, we can tentatively

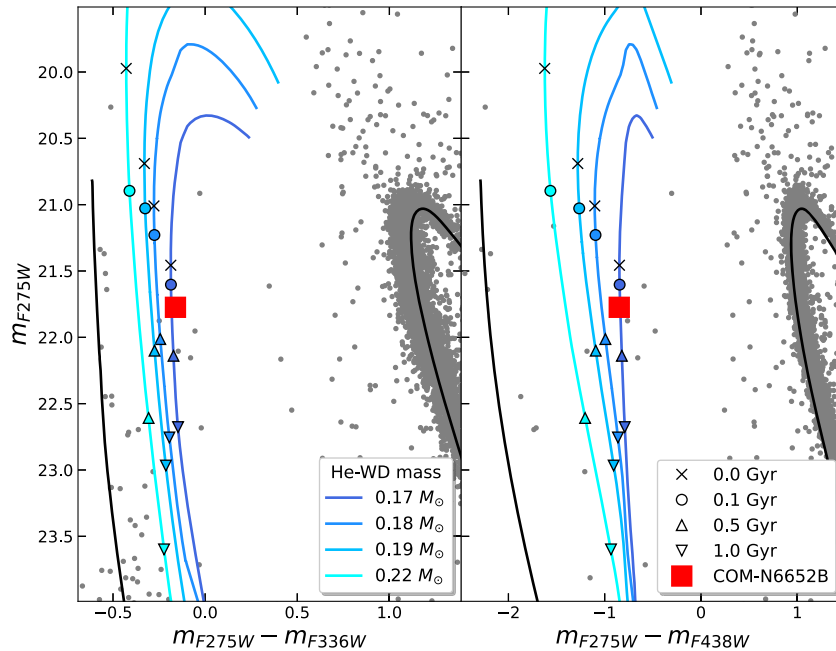


Figure 3. Same CMD as Figure 2, but the WD region is zoomed in. A theoretical cooling track of a $0.55 M_{\odot}$ CO-WD and an isochrone of 13.25 Gyr stellar population are marked with black lines, respectively. The other curves in color are cooling tracks of He-WD with masses of 0.17, 0.18, 0.19, and $0.22 M_{\odot}$, from left to right, where the cooling ages are marked with different symbols in tracks as reported in the legend.

hypothesize that the companion to NGC 6652B is a recently formed He-WD.

The adopted data set is composed of multiepoch observations. We investigated the magnitude of the counterpart in the different frames, but no evidence of photometric variability could be detected for the companion star. While this can be due to the poor sampling of the binary orbit, He-WD companions only rarely show variability, which is usually not related to the binary orbit but to stellar pulsations (e.g., Maxted et al. 2013; Kilic et al. 2015; Antoniadis et al. 2016a; Parsons et al. 2020). Indeed, heating and/or tidal distortions are negligible in the case of a WD companion (although exceptions exist; see, e.g., Edmonds et al. 2001; Kaplan et al. 2012), while they become significant in the case of nondegenerate and Roche lobe filling companions (e.g., Ferraro et al. 2001b; Pallanca et al. 2010, 2014; Cadelano et al. 2015a).

3.2. Comparison with Binary Evolution Models

In order to confirm the hypothesis that the companion to NGC 6652B is a He-WD and to derive its physical properties, we compared its position in the CMD with the prediction of theoretical binary evolution models. As a first step, we performed a calibration sanity check by comparing the observed standard evolutionary sequences (such as main-sequence and red giants) with an isochrone extracted from the BaSTI database (Hidalgo et al. 2018; Pietrinferni et al. 2021) with an age of 13.25 Gyr (Dotter et al. 2010), a metallicity $[\text{Fe}/\text{H}] = -0.8$ (Harris 1996, 2010 version), and $[\alpha/\text{Fe}] = +0.4$. We also compared the position of the observed WD cooling sequence with a theoretical cooling track extracted from the BaSTI database (Salaris et al. 2022) for CO-WDs with a canonical mass of $0.55 M_{\odot}$. Absolute magnitudes were converted to the observed frame by adopting a distance modulus of $(m - M)_0 = 14.97$ and a color excess of $E(B - V) = 0.1$ (in very good agreement with the values quoted

by Harris 1996) and using appropriate extinction coefficients from Cardelli et al. (1989) and O’Donnell (1994). As shown in Figure 3, both the isochrone and the CO-WD cooling track nicely reproduce the observed evolutionary sequences, thus confirming that the photometric calibration and cluster parameters are sufficiently precise to allow the next step of exploration.

In order to constrain the properties of the companion star, we extracted binary evolution models from the database described in Istrate et al. (2014, 2016). These models follow the evolution of an NS binary during the whole mass transfer stage, the proto-WD stage, and the WD cooling stage. The resulting evolution tracks cover a large parameter space with a He-WD mass range of $0.17\text{--}0.4 M_{\odot}$, a surface temperature of $5000\text{--}20,000$ K, and cooling ages¹¹ down to the cluster age. By using the Astrolib Pysynphot Package¹² (STScI Development Team 2013) and WD spectra templates (Tassoul et al. 1990; Tremblay & Bergeron 2009; Koester 2010), the theoretical bolometric luminosities were converted to the HST-WFC3 magnitudes. A selection of the evolutionary tracks are plotted in Figure 3. As expected, all the tracks are located along the red side of the CO-WD sequence. The CMD position of the companion star to NGC 6652B is nicely reproduced in both the filter combinations by the lowest available He-WD mass of $0.17 M_{\odot}$, thus confirming that the identified star is a He-WD. Unfortunately, the available evolutionary tracks do not properly cover the extreme He-WD low-mass end (for $M < 0.17 M_{\odot}$). This hampers a detailed characterization of the uncertainties (see Cadelano et al. 2019, 2020). However, the main physical properties of the companion star can be safely derived from the best-fit He-WD track mass ($0.17 M_{\odot}$) and

¹¹ Following Istrate et al. (2016), the WD cooling age is defined as the time passed since the proto-WD reached the maximum surface temperature along the evolutionary track.

¹² Pysynphot: <https://pysynphot.readthedocs.io/en/latest/>.

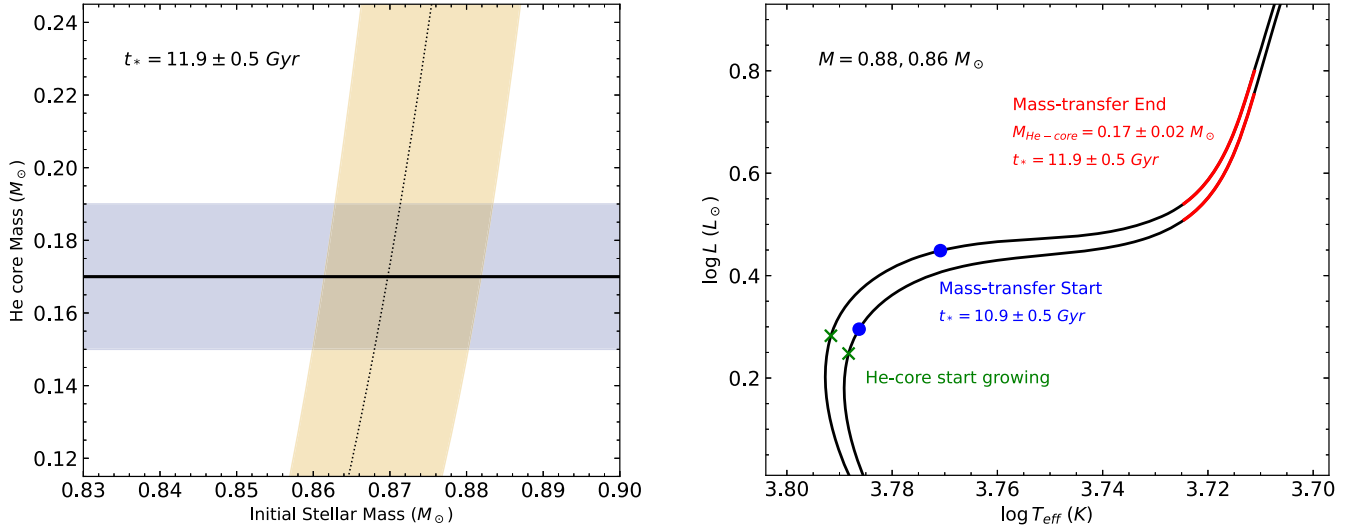


Figure 4. Left panel: He-core mass as a function of the stellar mass as predicted by the evolutionary tracks from PARSEC v2.0 (Costa et al. 2019a, 2019b; Nguyen et al. 2022). The black dashed curve and the light-orange shaded area represent the values for an age of 11.9 ± 0.5 Gyr, corresponding to the cluster age at the epoch of Roche lobe detachment. The horizontal line (and blue band) marks the mass of the He-WD companion to NGC 6652B. Right panel: the black curves are the evolutionary track for $0.88 M_{\odot}$ (left) and $0.86 M_{\odot}$ (right) stars. The red portion of the track highlights the phase where the star had a He core with a mass comparable to the one measured for the companion star. The blue circle marks the region of the tracks ~ 1 Gyr before the Roche lobe detachment when the mass transfer probably started. Finally, the green cross marks the region where the exhausted He core starts growing.

conservative uncertainties can be estimated through the available grid of higher mass tracks. In doing so the companion star turned out to have a mass of $0.17 \pm 0.02 M_{\odot}$, a surface gravity of $\log g = 5.7 \pm 0.3 \text{ cm s}^{-2}$, a surface temperature of $T_{\text{eff}} = 11,500 \pm 1900 \text{ K}$, and a very young age of only $200 \pm 100 \text{ Myr}$. This confirms that the companion to NGC 6652B is a recently formed He-WD. For such a He-WD, the proto-WD timescale, i.e., the time spent by the companion star from the Roche lobe detachment to the beginning of the cooling phase, is expected to last $1.2 \pm 0.2 \text{ Gyr}$. Although this value slightly depends also on the NS mass and companion metallicity, it suggests that the mass transfer phase in this system stopped around 1.4 Gyr ago, and then the companion went through a long bloated proto-WD stage in which a significant fraction of the hydrogen in the envelope was burned through stable burning, while the star contracted, eventually entering in the WD cooling sequence.

To further investigate the evolution of this system, we analyzed the growth rate of the He core of stars with different masses at the cluster metallicity extracted from the PARSEC v2.0 database (Costa et al. 2019a, 2019b; Nguyen et al. 2022). Assuming the cluster age of $13.25 \pm 0.5 \text{ Gyr}$ (Dotter et al. 2010), the sum of the companion cooling age and proto-WD age suggests that this system experienced the end of the mass transfer phase (i.e., Roche lobe detachment) when the cluster was $11.9 \pm 0.5 \text{ Gyr}$ old. Back then, only stars with masses between 0.86 and $0.88 M_{\odot}$ had sufficient time to grow a He core with a mass comparable to that of the companion star (see left panel of Figure 4). This poses a firm constraint of the mass of the progenitor companion star. Stars with mass in the range from 0.86 to $0.88 M_{\odot}$ have developed a $0.17 \pm 0.02 M_{\odot}$ He core during the very early stages of the red giant branch phase (see right panel of Figure 4). Assuming that the mass transfer phase lasted at most 1 Gyr, this process started when the companion star evolved to the subgiant branch stage.

3.3. Constraints on the NS Mass

With the determination of companion star mass, one can combine binary orbital parameters, derived through the radio timing, to constrain the mass of the NS from the mass function (Lyne & Graham-Smith 1998):

$$f(m_p, m_c, i) = \frac{4\pi^2 a^3 \sin^3 i}{G P_{\text{orb}}^2} = \frac{m_c^3 \sin^3 i}{(m_p + m_c)^2} \quad (1)$$

where m_p , m_c , are the NS and companion mass, respectively, i is the orbital inclination angle, a is the projected semimajor axis, and P_{orb} is the binary period. The above equation contains two unknown quantities, namely the NS mass and the orbital inclination angle. The NS mass as a function of the companion mass and inclination angles are shown in Figure 5, where it can be seen that the range of NS masses allowed by the known companion mass excludes the possibility of a high-mass NS. In fact, in the case of an edge-on binary, the NS mass is constrained between 1.1 and $1.6 M_{\odot}$. Lower inclination angles would result in lower NS mass ranges. In principle, a canonical mass NS of $M_{\text{NS}} = 1.4 M_{\odot}$ can be obtained with a large inclination angle of about $i = 80^\circ - 90^\circ$.

We also used a Markov Chain Monte Carlo sampler (Foreman-Mackey et al. 2019) to further constrain the mass and inclination angle of the MSP. Following Cadelano et al. (2020), we defined a Gaussian likelihood function to minimize the difference between the middle and right sides of Equation (1). We assumed a uniform prior on the distribution of $\cos i$ and also a prior on the NS mass distribution following the one derived by Antoniadis et al. (2016b). The posterior distribution is shown in Figure 6, and the results based on the 16th, 50th, and 84th percentiles show that NGC 6652B is likely an NS with a standard mass of $1.44 \pm 0.06 M_{\odot}$ in a binary seen with a large inclination angle. In fact, the probability

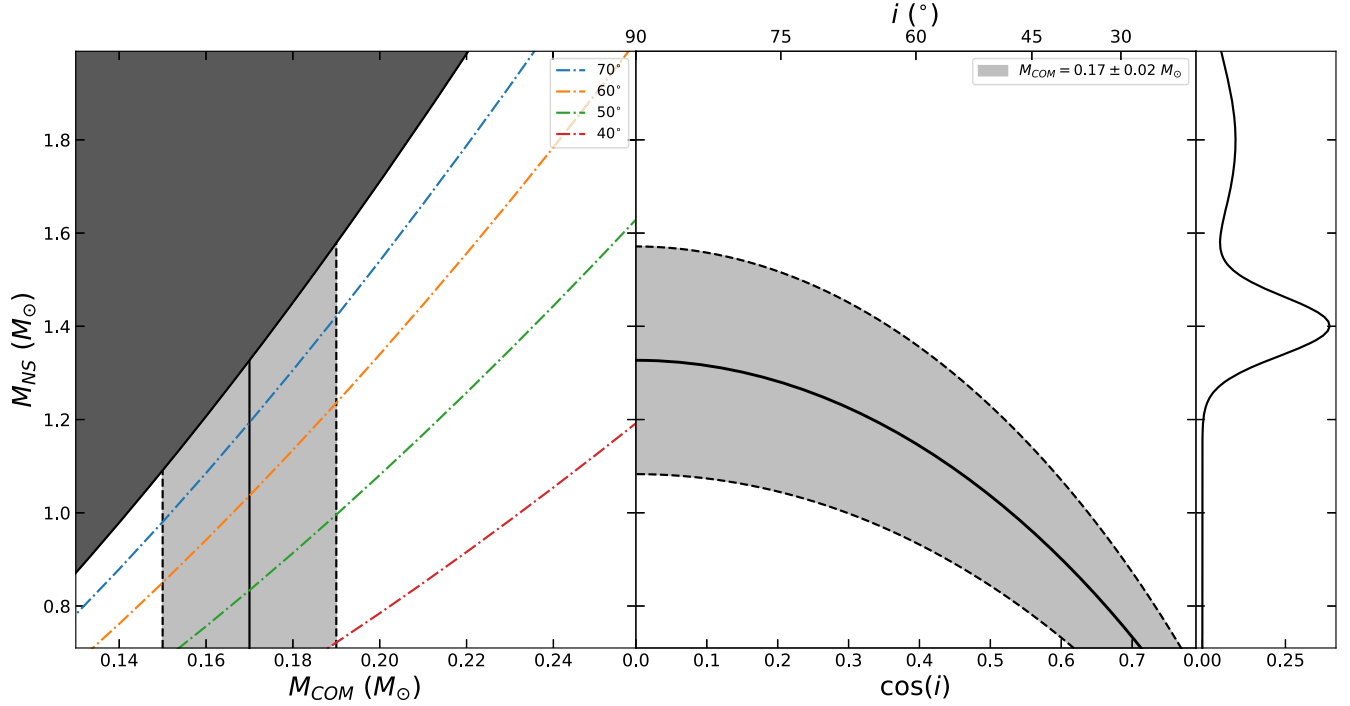


Figure 5. Left panel: NS mass as a function of the companion star mass. The best-fit value of the companion mass is marked with a solid vertical line, and the corresponding uncertainties are delimited by two dashed lines. The color dotted–dashed curves indicate the NS mass—companion mass relation at different inclination angles, while the shaded area is the region forbidden by the mass function. Right panel: NS mass as a function of the cosine of the inclination angle for the estimated mass of the companion star. The solid curve shows values predicted by the best-fit value of the companion mass, while the light-gray shaded region delimited by the two dashed curves shows the values allowed within the companion mass uncertainty. The rightmost panel shows, as a reference, the NS mass distribution empirically derived by Antoniadis et al. (2016b).

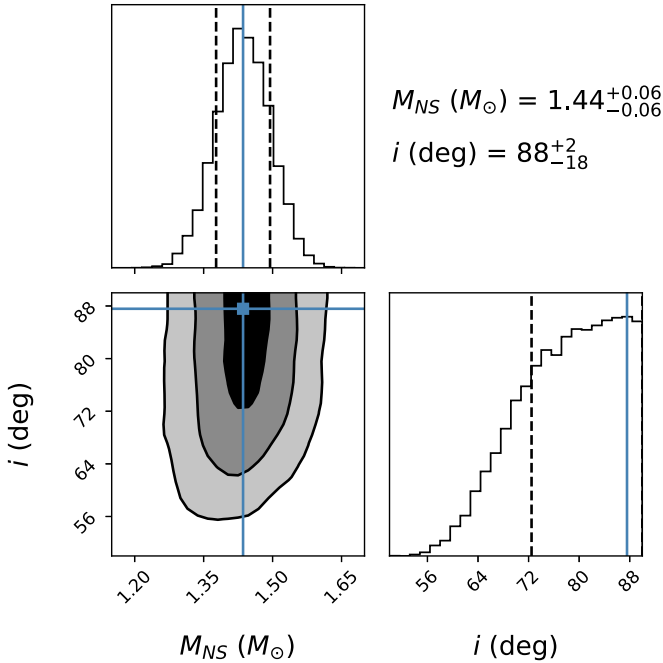


Figure 6. Constraints on the mass of the NS and the inclination angle of NGC 6652B. The 2D panel shows the posterior probability distribution of the two parameters, and the contours are the 1σ , 2σ , and 3σ confidence levels. The 1D histograms are the marginalized probability distributions of the two parameters, where the solid blue and black dashed lines are the best values and their related uncertainties, respectively.

distribution of the inclination angle reaches the maximum values for edge-on orbits. We therefore assumed that the best value for the inclination angle corresponds to the maximum in the probability distribution and its lower uncertainty to the 16th percentile: i (deg) = 88_{-18}^{+2} .

4. Conclusions

We used deep, high-resolution near-UV HST observations to study the binary MSPs in NGC 6652. By using the so-called “UV-route” approach, we searched for the companions to the binary MSPs in the cluster. At the corresponding position of NGC 6652B we found a blue object located along the red side of the brightest portion of the WD cooling sequence. This is a He-WD, i.e., the exhausted core of an evolving star that lost its envelope likely as a result of the mass transfer onto the NS. The comparison with binary evolution models revealed that the companion star is a newly formed He-WD with a cooling age of only 200 ± 100 Myr and a mass of $0.17 \pm 0.02 M_{\odot}$. The companion underwent a bloated proto-WD phase that lasted 1.2 ± 0.2 Gyr. Therefore, the Roche lobe detachment occurred ~ 1.4 Gyr ago, when the cluster was 11.9 Gyr old. The progenitor star of such a young and low-mass WD was likely a $\sim 0.87 M_{\odot}$ star that developed a He core with a mass of $0.17 M_{\odot}$ during the first stages of the evolution along the red giant branch, before the Roche lobe detachment. Therefore, the progenitor star lost $\sim 0.7 M_{\odot}$ during its evolution in the binary system. Assuming that the mass transfer stage lasted $\lesssim 1$ Gyr, it

begun when the progenitor star evolved along the subgiant branch phase, naturally increasing its radius owing to the standard stellar evolution, eventually filling its Roche lobe and starting the mass transfer onto the NS primary.

Combining together the companion mass here derived and the binary orbital properties derived through radio timing, we found that this system likely hosts an NS with a mass of $1.4 M_{\odot}$ seen at an almost edge-on orbit. The NS mass so derived is very similar to the canonical values expected and measured for these objects (e.g., Antoniadis et al. 2016b). Since the companion lost $\sim 0.7 M_{\odot}$ during the mass transfer, the derived NS mass suggests that the mass transfer phase was highly nonconservative. Future observations will improve the timing precision of this pulsar. Given the almost edge-on orbit predicted for this system, we expect a possible detection of the Shapiro delay in the future. Such a measurement will provide an independent estimate of the companion mass and orbital inclination angle, thus also granting a benchmark for binary evolution models.

As described by Gautam et al. (2022), NGC 6652B is an unusually bright pulsar, with the pulsed component representing only a small amount of the total emission. Such an unusual feature was inferred from the fact that the pulsar appears brighter in interferometric images than in the pulsed profile. The peculiarity of this system was further confirmed by Zhang et al. (2022). In fact, their detection of gamma-ray pulsations shows that this MSP is unusually energetic: it is only the third pulsar in a GC detected in gamma-rays, after NGC 6624A (Freire et al. 2011) and M28A (Johnson et al. 2013). From the orbital period derivative of the pulsar, Gautam et al. (2022) estimated the intrinsic spin-down of the pulsar $\dot{P}_{\text{int}} < 6.65 \times 10^{-20}$, corresponding to a characteristic age $\tau_c > 0.43$ Gyr and a gamma-ray efficiency of 0.12. The latter value indicates that \dot{P}_{int} cannot be much smaller than the derived upper limit; otherwise, the gamma-ray efficiency would be unreliably close to 1.0. This, in turns, means that τ_c cannot be much larger than the derived lower limit. All this suggests that NGC 6652B is an exceptionally young and powerful MSP, and the detection of the young WD companion presented in this

work is in perfect agreement with this scenario. The cooling age here derived is smaller than the characteristic age (assuming $\tau_c \sim 0.43$ Gyr). This is not surprising because τ_c is computed assuming that the initial spin period is much smaller than the current spin period, which is unlikely for an MSP with a short current spin period of 1.83 ms. For the much more probable case that the initial spin period was similar to what it is today, the real age of the pulsar is smaller than suggested by τ_c and more in agreement with the WD cooling age.

This work further confirms the strong and fruitful synergy between the new radio telescopes (such as MeerKat and FAST) and space telescopes (such as HST and JWST). Such a synergy allows a comprehensive view of the properties and evolution of binary MSPs in GCs through the observation of both the NS primaries in the radio bands and the companions in the optical bands.

This work is part of the project Cosmic-Lab at the Physics and Astronomy Department ‘‘A. Righi’’ of Bologna University (<http://www.cosmic-lab.eu/Cosmic-Lab/Home.html>). The research was funded by the MIUR throughout the PRIN-2017 grant awarded to the project Light-on-Dark (PI:Ferraro) through contract PRIN-2017K7REXT. J.C. acknowledges the support from the China Scholarship Council (CSC).

Facility: HST(WFC3).

Software: DAOPHOT(Stetson 1987), ALLFRAME(Stetson 1994), Pysynphot(STScI Development Team 2013), corner.py (Foreman-Mackey 2016), emcee(Foreman-Mackey et al. 2019).

Appendix PSR J1835–3259A

We carefully investigated the region surrounding the position of PSR J1835–3259A (NGC 6652A), but no stars are found at its corresponding position in the near-UV and optical images. Figure 7 shows the finding chart in the three WFC3 adopted filters. We also provide the magnitude upper limits of this system derived following Cadelano et al. (2015a): $m_{F275W} > 25.5$, $m_{F336W} > 25.5$, and $m_{F438W} > 23.0$.

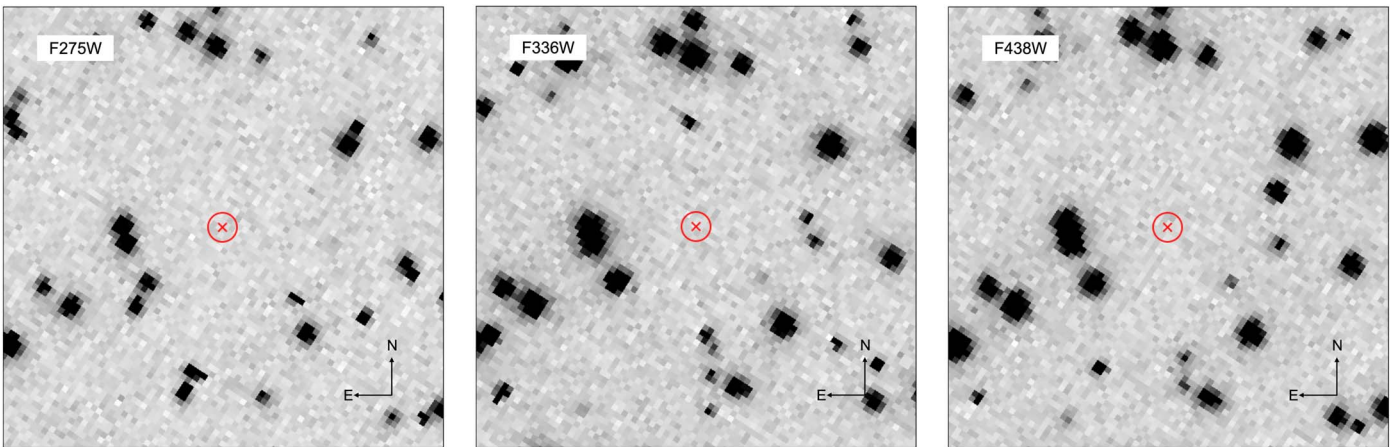
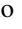
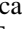
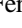
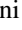




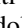


Figure 7. $3'' \times 3''$ finding chart of the region surrounding NGC 6652A in the F275W, F336W, and F438W filters. The red circle has a radius of 100 mas ($\sim 6\sigma$ uncertainty), while the center of the circle corresponds to the position of the MSP. No stars are detected at the pulsar corresponding position.

ORCID iDs

Jianxing Chen  <https://orcid.org/0000-0002-8004-549X>
 Mario Cadelano  <https://orcid.org/0000-0002-5038-3914>
 Cristina Pallanca  <https://orcid.org/0000-0002-7104-2107>
 Francesco R. Ferraro  <https://orcid.org/0000-0002-2165-8528>
 Barbara Lanzoni  <https://orcid.org/0000-0001-5613-4938>
 Alina G. Istrate  <https://orcid.org/0000-0002-8811-8171>
 Marta Burgay  <https://orcid.org/0000-0002-8265-4344>
 Paulo C. C. Freire  <https://orcid.org/0000-0003-1307-9435>
 Tasha Gautam  <https://orcid.org/0000-0002-8396-2197>
 Andrea Possenti  <https://orcid.org/0000-0001-5902-3731>
 Alessandro Ridolfi  <https://orcid.org/0000-0001-6762-2638>

References

- Ablimit, I., Podsiadlowski, P., Hirai, R., et al. 2022, *MNRAS*, 513, 4802
 Antoniadis, J., Kaplan, D. L., Stovall, K., et al. 2016a, *ApJ*, 830, 36
 Antoniadis, J., Tauris, T. M., Özel, F., et al. 2016b, arXiv:1605.01665
 Bellini, A., Anderson, J., & Bedin, L. R. 2011, *PASP*, 123, 622
 Belloni, D., Giersz, M., Rivera Sandoval, L. E., et al. 2019, *MNRAS*, 483, 315
 Belloni, D., Giersz, M., Sandoval, L. E. R., et al. 2020, in IAU Symp. 351, Star Clusters: From the Milky Way to the Early Universe (Cambridge: Cambridge Univ. Press), 404
 Bhattacharya, D., & van den Heuvel, E. P. J. 1991, *PhR*, 203, 1
 Cadelano, M., Chen, J., Pallanca, C., et al. 2020, *ApJ*, 905, 63
 Cadelano, M., Dalessandro, E., Ferraro, F. R., et al. 2017a, *ApJ*, 836, 170
 Cadelano, M., Ferraro, F. R., Dalessandro, E., et al. 2022, *ApJ*, 941, 69
 Cadelano, M., Ferraro, F. R., Istrate, A. G., et al. 2019, *ApJ*, 875, 25
 Cadelano, M., Pallanca, C., Ferraro, F. R., et al. 2015a, *ApJ*, 807, 91
 Cadelano, M., Pallanca, C., Ferraro, F. R., et al. 2015b, *ApJ*, 812, 63
 Cadelano, M., Pallanca, C., Ferraro, F. R., et al. 2017b, *ApJ*, 844, 53
 Cadelano, M., Ransom, S. M., Freire, P. C. C., et al. 2018, *ApJ*, 855, 125
 Cardelli, J. A., Clayton, G. C., & Mathis, J. S. 1989, *ApJ*, 345, 245
 Chen, J., Ferraro, F. R., Cadelano, M., et al. 2021, *NatAs*, 5, 1170
 Chen, J., Ferraro, F. R., Cadelano, M., et al. 2022, *ApJ*, 934, 93
 Cocozza, G., Ferraro, F. R., Possenti, A., et al. 2006, *ApJL*, 641, L129
 Costa, G., Girardi, L., Bressan, A., et al. 2019a, *A&A*, 631, A128
 Costa, G., Girardi, L., Bressan, A., et al. 2019b, *MNRAS*, 485, 4641
 Dalessandro, E., Ferraro, F. R., Massari, D., et al. 2013a, *ApJ*, 778, 135
 Dalessandro, E., Salaris, M., Ferraro, F. R., et al. 2013b, *MNRAS*, 430, 459
 DeCesar, M. E., Ransom, S. M., Kaplan, D. L., et al. 2015, *ApJL*, 807, L23
 Dotter, A., Sarajedini, A., Anderson, J., et al. 2010, *ApJ*, 708, 698
 Douglas, A., Padmanabh, P. V., Ransom, S. M., et al. 2022, *ApJ*, 927, 126
 Driebe, T., Schoenberner, D., Bloeker, T., et al. 1998, *A&A*, 339, 123
 Edmonds, P. D., Gilliland, R. L., Heinke, C. O., et al. 2001, *ApJL*, 557, L57
 Ferraro, F. R., Beccari, G., Dalessandro, E., et al. 2009, *Natur*, 462, 1028
 Ferraro, F. R., Beccari, G., Rood, R. T., et al. 2004, *ApJ*, 603, 127
 Ferraro, F. R., D'Amico, N., Possenti, A., et al. 2001a, *ApJ*, 561, 337
 Ferraro, F. R., Lanzoni, B., Dalessandro, E., et al. 2012, *Natur*, 492, 393
 Ferraro, F. R., Lanzoni, B., Dalessandro, E., et al. 2019, *NatAs*, 3, 1149
 Ferraro, F. R., Lanzoni, B., & Dalessandro, E. 2020, *RLSFN*, 31, 19
 Ferraro, F. R., Lanzoni, B., Raso, S., et al. 2018, *ApJ*, 860, 36
 Ferraro, F. R., Pallanca, C., Lanzoni, B., et al. 2015, *ApJL*, 807, L1
 Ferraro, F. R., Paltrinieri, B., Fusi Pecci, F., et al. 1997a, *A&A*, 324, 915
 Ferraro, F. R., Paltrinieri, B., Fusi Pecci, F., et al. 1997b, *ApJL*, 484, L145
 Ferraro, F. R., Paltrinieri, B., Rood, R. T., et al. 1999, *ApJ*, 522, 983
 Ferraro, F. R., & Paresce, F. 1993, *AJ*, 106, 154
 Ferraro, F. R., Pecci, F. F., Cacciari, C., et al. 1993, *AJ*, 106, 2324
 Ferraro, F. R., Possenti, A., D'Amico, N., et al. 2001b, *ApJL*, 561, L93
 Ferraro, F. R., Possenti, A., Sabbi, E., et al. 2003a, *ApJL*, 596, L211
 Ferraro, F. R., Sills, A., Rood, R. T., et al. 2003b, *ApJ*, 588, 464
 Foreman-Mackey, D. 2016, *JOSS*, 1, 24
 Foreman-Mackey, D., Farr, W., Sinha, M., et al. 2019, *JOSS*, 4, 1864
 Freire, P. C. C., Abdo, A. A., Ajello, M., et al. 2011, *Sci*, 334, 1107
 Freire, P. C. C., Ridolfi, A., Kramer, M., et al. 2017, *MNRAS*, 471, 857
 Freire, P. C. C., & Tauris, T. M. 2014, *MNRAS*, 438, L86
 Gaia Collaboration, Vallenari, A., Brown, A. G. A., et al. 2022, arXiv:2208.00211
 Gautam, T., Ridolfi, A., Freire, P. C. C., et al. 2022, *A&A*, 664, A54
 Harris, W. E. 1996, *AJ*, 112, 1487
 Hidalgo, S. L., Pietrinferni, A., Cassisi, S., et al. 2018, *ApJ*, 856, 125
 Istrate, A. G., Marchant, P., Tauris, T. M., et al. 2016, *A&A*, 595, A35
 Istrate, A. G., Tauris, T. M., Langer, N., et al. 2014, *A&A*, 571, L3
 Johnson, T. J., Guilletot, L., Kerr, M., et al. 2013, *ApJ*, 778, 106
 Kaplan, D. L., Stovall, K., Ransom, S. M., et al. 2012, *ApJ*, 753, 174
 Kilic, M., Hermes, J. J., Gianninas, A., et al. 2015, *MNRAS*, 446, L26
 Koester, D. 2010, *MmSAI*, 81, 921
 Lanzoni, B., Ferraro, F. R., Dalessandro, E., et al. 2019, *ApJ*, 887, 176
 Lattimer, J. M. 2012, *ARNPS*, 62, 485
 Libralato, M., Bellini, A., Vesperini, E., et al. 2022, *ApJ*, 934, 150
 Lyne, A. G., Brinklow, A., Middleditch, J., et al. 1987, *Natur*, 328, 399
 Lyne, A. G., & Graham-Smith, F. 1998, in Pulsar Astronomy, ed. A. G. Lyne & F. Graham-Smith (Cambridge: Cambridge Univ. Press)
 Maxted, P. F. L., Serenelli, A. M., Miglio, A., et al. 2013, *Natur*, 498, 463
 Mucciarelli, A., Salaris, M., Lanzoni, B., et al. 2013, *ApJL*, 772, L27
 Nguyen, C. T., Costa, G., Girardi, L., et al. 2022, *A&A*, 665, A126
 Nomoto, K. 1987, *ApJ*, 322, 206
 O'Donnell, J. E. 1994, *ApJ*, 422, 158
 Özel, F., & Freire, P. 2016, *ARA&A*, 54, 401
 Pallanca, C., Dalessandro, E., Ferraro, F. R., et al. 2010, *ApJ*, 725, 1165
 Pallanca, C., Dalessandro, E., Ferraro, F. R., et al. 2013, *ApJ*, 773, 122
 Pallanca, C., Ransom, S. M., Ferraro, F. R., et al. 2014, *ApJ*, 795, 29
 Parsons, S. G., Brown, A. J., Littlefair, S. P., et al. 2020, *NatAs*, 4, 690
 Pietrinferni, A., Hidalgo, S., Cassisi, S., et al. 2021, *ApJ*, 908, 102
 Ransom, S. M., Hessels, J. W. T., Stairs, I. H., et al. 2005, *Sci*, 307, 892
 Raso, S., Ferraro, F. R., Dalessandro, E., et al. 2017, *ApJ*, 839, 64
 Raso, S., Libralato, M., Bellini, A., et al. 2020, *ApJ*, 895, 15
 Ridolfi, A., Freire, P. C. C., Gautam, T., et al. 2022, *A&A*, 664, A27
 Rivera Sandoval, L. E., van den Berg, M., Heinke, C. O., et al. 2018, *MNRAS*, 475, 4841
 Roberts, M. S. E. 2013, in IAU Symp. 291, Neutron Stars and Pulsars: Challenges and Opportunities after 80 years (Cambridge: Cambridge Univ. Press), 127
 Sabbi, E., Gratton, R., Ferraro, F. R., et al. 2003a, *ApJL*, 589, L41
 Sabbi, E., Gratton, R. G., Bragaglia, A., et al. 2003b, *A&A*, 412, 829
 Salaris, M., Cassisi, S., Pietrinferni, A., et al. 2022, *MNRAS*, 509, 5197
 Stetson, P. B. 1987, *PASP*, 99, 191
 Stetson, P. B. 1994, *PASP*, 106, 250
 STScI Development Team 2013, pysynphot: Synthetic photometry software package, Astrophysics Source Code Library, ascl: 1303.023
 Tassoul, M., Fontaine, G., & Winget, D. E. 1990, *ApJS*, 72, 335
 Tauris, T. M., Kramer, M., Freire, P. C. C., et al. 2017, *ApJ*, 846, 170
 Tauris, T. M., Sanyal, D., Yoon, S.-C., et al. 2013, *A&A*, 558, A39
 Tauris, T. M., & Savonije, G. J. 1999, *A&A*, 350, 928
 Tremblay, P.-E., & Bergeron, P. 2009, *ApJ*, 696, 1755
 Wang, B., Liu, D., & Chen, H. 2022, *MNRAS*, 510, 6011
 Wijnands, R., & van der Klis, M. 1998, *Natur*, 394, 344
 Zhang, P., Xing, Y., & Wang, Z. 2022, *ApJL*, 935, L36